**Atmospheric
Chemistry
and Physics
Discussions**

Seasonal cycle and source analyses of aerosol optical properties in a semi-urban environment at Puijo station in Eastern Finland

A. Leskinen[1], A. Arola[1], M. Komppula[1], H. Portin[1,2], P. Tiitta[2,3], P. Miettinen[2], S. Romakkaniemi[2], A. Laaksonen[2,4], and K. E. J. Lehtinen[1,2]

[1]Finnish Meteorological Institute, Kuopio Unit, P.O. Box 1627, 70211 Kuopio, Finland
[2]University of Eastern Finland, Department of Applied Physics, P.O. Box 1627, 70211 Kuopio, Finland
[3]Atmospheric Chemistry Research Group, North-West University, Potchefstroom 2520, South Africa
[4]Finnish Meteorological Institute, Research and Development, P.O. Box 503, 00101 Helsinki, Finland

Correspondence to: A. Leskinen (ari.leskinen@fmi.fi)

Seasonal cycle and source analyses of aerosol optical properties

A. Leskinen et al.

Title Page

Abstract	Introduction
Conclusions	References
Tables	Figures

|◄| |►|
|◄| |►|

Back | Close

Full Screen / Esc

Printer-friendly Version

Interactive Discussion

Full Screen / Esc

Abstract

We introduce a four-year (2006–2010) continuous data set of aerosol optical properties at Puijo in Kuopio, Finland. We study the annual and diurnal variation of the aerosol scattering and absorption coefficients, hemispheric backscattering fraction, scattering Ångström exponent, and single scattering albedo, whose averages over this period were 11.1 Mm^{-1} (at 550 nm), 1.5 Mm^{-1} (at 670 nm), 0.13, 1.9, and 0.83, respectively. The scattering coefficient peaked in the spring and autumn, being 2–4 times those in the summer and winter. An exception was the summer of 2010, when the the scattering coefficient was elevated to ~300 Mm^{-1} by the plumes from forest fires in Russia. The absorption coefficient peaked in the winter with values of 2–3 times those in the summer. The single scattering albedo was lowest in the winter when more biomass burning derived, soot-containing aerosols were present. The optical properties varied also with wind direction and time of the day, indicating the effect of the local pollutant sources and the age of the particles. Peak values in the single scattering albedo were observed when the wind blew from a paper mill and from the sector without local pollutant sources. These observations were linked to the sulphate-rich aerosol from the paper mill and the oxygenated organics in the aged aerosol, which both are known to increase the scattering characteristics of aerosols. Changes in the single scattering albedo in the morning and afternoon in the summertime were linked to the increased traffic density at these hours. The scattering and absorption coefficients were found to be decreased by clouds. The effect was stronger for the scattering than absorption, indicating preferential activation of the more hygroscopic aerosol with higher scattering characteristics. What happens to the aerosol optical properties during a cloud event when the air masses come from different directions with different local sources, is under a more detailed inspection. Also, more aerosol mass spectrometry data will be analyzed in order to strengthen our knowledge about the role of the chemical composition of the aerosol particles in their activation into cloud droplets.

1   Introduction

According to the Intergovernmental Panel on Climate Change the direct effect of aerosols to radiative forcing has still a great uncertainty (IPCC, 2007). The direct effect arises from light extinction by aerosol particles, i.e. light scattering from and absorption to the aerosols. Evaluation of its magnitude is complicated, because these proper-ties depend on the wavelength of the incident light and the angular distribution of the scattered light, which, in turn, depends, e.g., on the size, concentration, and chemical composition of the aerosol particles. Particles that contain sulfate, nitrate, and organic carbon, predominately scatter light, and particles that contain black carbon, absorb it. Furthermore, internal mixing of e.g. organics and black carbon may influence dramati-cally the aerosol optical properties (Shiraiwa et al., 2010).

The optical properties of aerosol particles are usually retrieved from remote sens-ing instruments, such as an automated Polly^{XT} Lidar, i.e. Light detection and ranging (Althausen et al., 2009), or from in-situ instruments, either airborne (Shinozuka et al., 2011; Chen et al., 2011) or ground-based (Virkkula et al., 2011). The extinction can be measured, e.g., with a pulsed cavity ring-down spectrometer (Baynard et al., 2007), scattering with nephelometers (Heintzenberg et al., 1996; Anderson et al., 1996), and absorption with photometers (Petzold and Schönlinner 2004; Arnott et al., 1999). Other important, so called extensive properties, such as the single scattering albedo (SSA), can be derived from the measured values. The SSA can be used to determine whether an aerosol layer causes net heating or cooling. If multi-wavelength instruments are used, so called Ångström exponents (å) can be derived for scattering (å$_s$) and ab-sorption (å$_a$). The å$_s$ depend inversely on the size of the aerosol particles: A small å value indicates large aerosol particles, such as sea salt and dust, whereas a larger å is connected to smaller aerosol particles (Bohren and Huffman, 1983), originating, for example, from combustion processes.

Measurements of aerosol optical properties have been conducted worldwide. Long-term measurements have been carried out in anthropogenically influenced continental

and coastal areas (Delene and Ogren, 2002) and more recently in remote areas in a boreal forest (Virkkula et al., 2011) and at elevated altitudes (Aaltonen et al., 2006; Hyvärinen et al., 2009; Marcq et al., 2010). Measurement campaigns have been conducted e.g. in an urban environment (He et al., 2009), at coastal sites (Fischer et al.,
5 2010; Pandolfi et al., 2011), and in the Arctic (Zieger et al., 2010). In most studies, particle size and concentration have been coupled to the aerosol optical properties, but, for example, the chemical composition and the optical properties of aerosols have been analyzed in parallel only in few studies.

In this study we introduce a previously unpublished four-year data set of aerosol opti-
10 cal properties and meteorological parameters measured at a semi-urban measurement station, 230 m above the surroundings, in an observation tower at Puijo in Kuopio, Finland (Leskinen et al., 2009). We interpret the annual and diurnal variation of the aerosol scattering and absorption coefficients, single scattering albedo, scattering Ångström exponent and hemispheric backscattering fraction. We classify the optical properties,
15 as well as aerosol chemical composition obtained from aerosol mass spectrometry, according to the wind direction in order to inspect the effect of the local sources. Furthermore, we examine how the scattering and absorption coefficients behave before, during, and after a cloud event, i.e. a time period when the station was covered by clouds.

20 ## 2 Methods

2.1 Site description

The measurement station at Puijo (62°54′32″ N, 27°39′31″ E) is on the top of an observation and retransmitting tower, which is a 75 m high building on the Puijo hill (elevation 150 m), approximately 2 km northwest of the city center of Kuopio. The measurements
25 are carried out at the height of 306 m a.s.l. and 224 m above the surrounding lake level. The surroundings of the Puijo hill belongs to the southern boreal climatic zone and is

characterized by forests with conifer (mostly pine and spruce) and deciduous (mostly birch) trees, an undulating terrain with rocky soil and moderate height hills, and lots of long lakes in the northwest-southeast direction.

We categorize the Puijo measurement station as a semi-urban measurement station, because there are local pollutant sources (traffic routes, residential areas, industrial plants) in a particular sector (0–245°) seen from the Puijo tower, whereas the remaining sector (245–360°) represents a "cleaner" sector with almost no local sources. This enables studying the effects of fresh emissions on various aerosol properties (Leskinen et al., 2009). Furthermore, its elevated location enables studies of the interaction of aerosols with low-level clouds (Portin et al., 2009).

Since its establishment in 2005 by the research groups at the Finnish Meteorological Institute in Kuopio and Helsinki and at the University of Eastern Finland (Kuopio), we have instrumented the station for continuous measurements of aerosols, cloud droplets, weather parameters and trace gases. In 2009, the Puijo measurement station became a part of the Station for Measuring Forest Ecosystem – Atmosphere Relations network as its fourth member (SMEAR IV). More details about the measurement station and an overview of the activities in its early stages are given in Leskinen et al. (2009) and Portin et al. (2009).

2.2 Instrumentation

We measured the meteorological parameters (temperature, relative humidity, atmospheric pressure, horizontal wind speed and direction, visibility and precipitation intensity and type) on the roof of the Puijo tower with a time resolution of 1 min. The temperature and relative humidity transmitters, and the ultrasonic wind anemometer (Thies UA2D) are 2 m and 5 m above the roof, respectively. The present weather sensor (Vaisala FD12P) and a weather camera, facing northwards, are attached to a vertical pole at 2 m height.

The aerosol instruments are located in the space below the roof of the tower. The samples to the instruments are drawn through two parallel sampling lines: one, called

A. Leskinen et al.

the interstitial inlet and sampling line, is equipped with an impactor with a 10-µm cut-off size, followed by a cyclone with a 2.5-µm cut-off size (1.0 µm since 20 November 2009), and the other, called the total air inlet and sampling line, with a heated inlet and snow-hood in order to dry the cloud droplets. The total air inlet has the same construction as that used and designed by Weingartner et al. (1999), who reported that the cut-off size of the inlet is 40 µm when the wind speed is below $20\,\mathrm{m\,s^{-1}}$, which is the case most of the time at Puijo. This two-inlet setup enables simultaneous in-cloud and out-of-cloud measurements when the tower is covered by clouds.

We measured the aerosol total and backscattering coefficients at 450 nm ($\sigma_{\mathrm{sp},450}$ and $\sigma_{\mathrm{bsp},450}$), 550 nm ($\sigma_{\mathrm{sp},550}$ and $\sigma_{\mathrm{bsp},550}$), and 700 nm ($\sigma_{\mathrm{sp},700}$ and $\sigma_{\mathrm{bsp},700}$) by using an integrating nephelometer (TSI Model 3563) (e.g., Anderson et al., 1996). The neph-elometer illuminates the sample volume from the side and detects the light scattered by the aerosol particles and gas molecules in the sample with a photomultiplier tube over an angle of 7–170°. The backscattering is measured, when a shutter blocks the light scattered to over 90° angles. The nephelometer was drawing the sample out of the cloud interstitial sample line with a flow rate of $10\,\mathrm{l\,min^{-1}}$ ($8.0\,\mathrm{l\,min^{-1}}$ since 8 October 2009). We checked the nephelometer calibration periodically with pure carbon dioxide and filtered air.

We measured the aerosol absorption with a multi-angle absorption photometer (Thermo Model 5012 MAAP). The MAAP (Petzold and Schönlinner, 2004) determines aerosol light absorption by illuminating a particle-loaded filter with 670 nm light and measuring simultaneously the radiation passing through the filter. It also measures the light scattered from the filter at several detection angles in order to resolve the influence of aerosol components that scatter light on the back-scattered radiation. This compensation of light-scattering effects improves considerably the aerosol absorption measurement in filter-based appliances. The MAAP was connected to the interstitial sample line and the flow rate through it was $5.0\,\mathrm{l\,min^{-1}}$. We performed periodic checks and flow calibrations for the instrument.

The MAAP provides the absorption information as an equivalent black carbon concentration (EBC), which is obtained by dividing the measured absorption coefficient by a mass absorption coefficient (MAC) of $6.6\,\mathrm{m^2\,g^{-1}}$, recommended by the manufacturer. To obtain the absorption coefficient ($\sigma_{ap,670}$), we multiplied the EBC by the same MAC ($6.6\,\mathrm{m^2\,g^{-1}}$). It must be noted that the MAC for a specific aerosol can vary during its lifetime and due to changes in its chemical composition, which causes uncertainty in the EBC, if a constant value of MAC is used. For example, values ranging from 6.9–$11.6\,\mathrm{m^2\,g^{-1}}$ have been reported (Knox et al., 2009; Pandolfi et al., 2011). However, as we used the the same MAC value as the MAAP in our calculation, we consider that the variability in MAC as a source of uncertainty can be neglected.

We analyzed the chemical composition of the aerosols in an intensive campaign 16 September–20 October 2008 by using aerosol mass spectrometry (AMS). The AMS reveals the chemical composition of Aitken and accumulation mode aerosol particles online and in real time. The particles are introduced into the AMS through a critical orifice and an aerodynamic lens assembly, producing a narrow aerosol beam that enters an ionization chamber, where non-refractory components flash-vaporize and positive ions are detected by Quadrupole mass spectrometer (Q-AMS). A more detailed description of the instrument is given by Jayne et al. (2000). The AMS used in this study gave the concentration of sulphate and organics, and the ratio of *m/z* 44 to *m/z* 43, which indicates the degree of oxygenation of organics: the higher the ratio, the more oxygenated the organics.

2.3 Data processing

We analyzed the nephelometer and MAAP data covering the time range 1 September 2006–30 September 2010. First we ruled out the unusable data due to abnormal peaks, calibrations, maintenance, flow checks, and autozeroing, and omitted the data with the relative humidity higher than 40 % in the nephelometer inlet, because the increasing water content increases the scattering coefficient (Fierz-Schmidhauser

A. Leskinen et al.

Title Page

Abstract	Introduction
Conclusions	References
Tables	Figures

◄◄ | ►►

◄ | ►

Back | Close

Full Screen / Esc

Printer-friendly Version

Interactive Discussion

et al., 2010) too much compared to dry particles, which we wanted to inspect. We also rejected the scattering coefficients below the detection limits given by Anderson et al. (1996). We then corrected the valid measured scattering coefficients for truncation errors arising from the physical limitations of the nephelometer (the actual measuring angle is 7–170°, not 0–180°), by using the values for no cut at the inlet, given by Anderson and Ogren (1998), and normalized them to standard temperature and pressure (273.15 K and 101 325 Pa), as described, e.g., in Hänel (1998).

We calculated hourly averages of the valid data for each instrument and used them in the following data analysis. Based on the scattering and absorption coefficients we calculated three intensive properties: the hemispheric backscattering fraction (b), scattering Ångström exponent ($å_s$), and the single scattering albedo (SSA). All three are dimensionless and independent of the amount of particles. The b is the ratio of aerosol scattering to the backward hemisphere to the scattering in all directions, and can be used to estimate, how much of the incoming solar radiation is reflected backwards.

We calculated the b at the wavelengths of 450, 550 and 700 nm for the periods 1 September–30 November 2006 and 1 November–30 September 2010. At other times the backscatter mode in the nephelometer was inactive. We calculated the $å_s$ for each pair of wavelengths: 700 and 450 nm ($å_{s,700-450}$), 700 and 550 nm ($å_{s,550-450}$), and 550 and 450 nm ($å_{s,550-450}$) by using the equation $å_{s,\lambda1-\lambda2} = -[\log(\sigma_{sp,\lambda1}/\sigma_{sp,\lambda2})/\log(\lambda_1/\lambda_2)]$. The scattering data with a negative $å_s$ were ruled out.

The SSA is defined as the ratio of the scattering coefficient to the extinction coefficient (the sum of the scattering and absorption coefficients) at a certain wavelength. Since the wavelengths of the nephelometer and MAAP unmatch, we determined the scattering coefficient at 670 nm ($\sigma_{sp,670}$) by using the Ångström power law, $\sigma_{sp,670} = \sigma_{sp,550}* (550/670)^{-å_{s,700-450}}$, where the scattering Ångström exponent $å_{s,\,700-450}$ was calculated from the scattering coefficients at 450 and 700 nm. The SSA at 670 nm was then calculated as $SSA_{670} = \sigma_{sp,670}/(\sigma_{ap,670} + \sigma_{sp,670})$, where $\sigma_{ap,670}$ is the absorption coefficient at 670 nm.

We calculated monthly averages for the scattering and absorption coefficients and the SSA, and sorted the data for each month in order to calculate the 10th and 90th percentiles as an indicator for the variability of the parameter values each month. We excluded rainy periods with a precipitation intensity more than $0.2\,\mathrm{Mm\,h^{-1}}$, whose oc-
5 currence was, on an average, 11 % of the time. We also excluded cloudy periods lasting more than 15 min (4 % of the valid data), i.e. the periods when the tower was covered by low-level clouds. The presence of a cloud was indicated by a sudden drop in the horizontal visibility below 200 m and a burst in cloud droplet concentration measured by a Cloud Droplet Probe (Portin et al., 2009).
10 In order to examine the effect of cloud events on the aerosol optical properties we separated the optical properties measured from the interstitial and total sampling lines for a four-day period (7–11 October 2010). For this special case, the nephelometer and MAAP were connected to a four-valve system, which changes the sampling inlets of the instruments in 6-min cycles. During the cycle 1 the MAAP was connected to
15 the interstitial line and the nephelometer to the total air line and during the cycle 2 vice versa. In this setup the MAAP flow was increased to $8.0\,\mathrm{l\,min^{-1}}$ in order to maintain equal flow rates in both inlets.

2.4 Local source analysis

We divided the measured and calculated parameters according to the prevailing wind
20 direction into (1) equal, 22.5-degree sectors and (2) five sectors described below, in order to analyse the effect of the local pollutant sources. Furthermore, we analyzed the monthly data as a function of the hour in order to see possible diurnal variation, e.g., as a consequence of the time-dependent sources, such as the traffic. The major point sources around Puijo are a paper mill (5 km in the direction of 35°) and a district heating
25 plant (3.5 km, 160°). A distinct line source, the Route 5/E63 highway, runs from north (6°) to south (192°). The most important area sources are the eastern residential areas (1.2–4.0 km in the sector of 45–120°), the city center (1.6–3.2 km, 120–155°), the southern residential areas (3.4–10 km, 155–245°), and the western residential areas

(1.5–3.5 km, 245–360°). Based on the distances and bearings of the pollutant sources, the chosen sectors were (1) 0–45°, including the northern highway and the paper mill, (2) 45–155°, including the city center and the eastern residential areas, extending up to 4 km, (3) 155–215°, including the district heating plant and the southern residential areas extending up to 10 km, (4) 215–245°, including the southern residential areas extending up to 4 km, and (5) 245–360°, including the western residential areas, extending up to 1–3 km.

It must be noted that the measurements were made approximately 230 m above the release height of the traffic and domestic emissions, which are diluted before they reach the measurement point. Furthermore, if mixing is inefficient the emissions from the very nearby sources might pass under the measurement point and would not be observed.

2.5 Trajectory analysis

In order to reveal the air mass arrival patterns, we calculated 120-h backward trajectories for the period from September 2006 to September 2010 in three-hour intervals, by using FLEXTRA trajectory model (Stohl et al., 1995). We classified the trajectories into five air mass arrival sectors, named as Arctic (315–10°), Arctic/Kola (10–70°), East (70–160°), South (160–235°) and West (235–315°). The East and South sectors represent the continental air/sources from Russia and Europe, respectively. The West sector covers the Northern Atlantic and the Arctic sector the Arctic Ocean. We furthermore divided the Arctic sector into two sectors in order to separate the Kola Peninsula sources from the clean Arctic air. We classified each trajectory according to its main sector, i.e. the sector where it had spent most of the time during the last 120 h. It must be noted that these sectors do not match with the wind direction sectors determined by the local pollutant sources. Therefore, we calculated, for each local source sector, the percentages of time that the air masses had spent in each long-range transport sector before arriving at Puijo.

3   Results and discussion

3.1   Meteorological parameters

The temperature, relative humidity and horizontal visibility had, as expected, clear seasonal cycles (Fig. 1), with averages over the four-year period of 3.2 °C, 80 % RH, and 28 km. February 2007 and January–February 2010 were found exceptionally cold sub-periods, with average temperatures of −12.8 °C and −12.5 °C, and minimum temperatures of −22.6 °C and −27.4 °C, respectively. The July 2010 was, in turn, exceptionally warm throughout the Eastern Europe (Barriopedro et al., 2011), with a maximum hourly average of 32.9 °C at Puijo.

3.2   Aerosol scattering and absorption

During the measurement period (2006–2010) the average, based on 20 175 hourly observations of the total scattering coefficients at 450, 550, and 700 nm, were 16.4, 11.1, and 6.8 Mm^{-1}, respectively (Table 1). The $\sigma_{sp,550}$ is approximately 1.5–6 times that observed in the Arctic region (Delene and Ogren, 2002; Aaltonen et al., 2006; Zieger et al., 2010). The long-time average for the $\sigma_{ap,670}$ at Puijo was 1.5 Mm^{-1}, which corresponds to a black carbon concentration of 9.9 ng m^{-3}. This is 4 times the average absorption coefficient of 0.36 Mm^{-1} and comparable to the BC concentration of 7.2 ng m^{-3} in the Arctic region, observed by Delene and Ogren (2002) and Zieger et al. (2010), respectively. This together with the comparatively low $\sigma_{sp,550}$ puts Puijo into a relatively clean class, when regarding the aerosol optical properties. However, as we will discuss in Sect. 3.4., the aerosol scattering and absorption coefficients at Puijo reach occasionally comparable values to those in the highly polluted areas, where scattering coefficients ranging up to ∼500 Mm^{-1} and absorption coefficients ∼100 Mm^{-1} have been observed (Bergin et al., 2001; Li et al., 2007; Andreae et al., 2008).

The monthly average of $\sigma_{sp,550}$ had a distinct seasonal cycle, being at its lowest in the summer and winter and at its highest in the spring and autumn (Fig. 2a). The seasonal

variation was similar also at 450 nm and 700 nm. The summer of 2010 made an exception to this pattern, because long-transported aerosol from forest fires in Russia increased the total scattering coefficients to over 20-fold of the normal summer values during the most smoky episodes (Portin et al., 2012). The maximum hourly average (352 Mm^{-1}) was observed in August 2010. The gaps in the data in Figure 2a are due to maintenance of the instrument or its visit to another measurement site.

The average of the backscattering coefficient at 450, 550, and 700 nm was 3.3, 2.3, and 2.3 Mm^{-1} for the 11 months when its measurement was active. This results, for example, as an average (± 1 standard deviation) hemispheric backscattering fraction of (0.13 ± 0.04) at 550 nm. For the backscattering coefficient at 550 nm (Fig. 2b) a seasonal trend cannot be stated due to inactive backscatter mode in the nephelometer between 1 December 2006–31 October 2009, but overall the monthly average of the hemispheric backscatter fraction varied between 0.10–0.15 (Fig. 3a). The *b* measured at Puijo corresponds to the values measured at various places (Delene and Ogren 2002; Aaltonen et al., 2006; Virkkula et al., 2011).

The $\sigma_{\mathrm{ap,670}}$ peaked in the early spring, when the monthly average was, depending on the year, 2.2–3.2 Mm^{-1} (Fig. 2c). The maximum of the hourly averages, 36 Mm^{-1}, was observed in January 2008. The lowest values occurred in the summer, when the average was 0.8–1.0 Mm^{-1}. The 2–3 fold values in the early spring are likely connected to inversion episodes coupled to inefficient mixing of the boundary layer and increased biomass burning in domestic combustion appliances, which produces, among others, particles that contain more black carbon, a good absorber of light. The seasonal variation – as well as the long-term statistics – of $\sigma_{\mathrm{ap,670}}$ was similar to that observed, 200 km from Puijo in Hyytiälä (Virkkula et al., 2011).

The long-transported aerosol from forest fires in Russia in July–August 2010 did not increase the $\sigma_{\mathrm{ap,670}}$ as much as the scattering coefficients, which could be explained by the domination of aged aerosol particles with less absorptive constituents during the smoke episodes. On the contrary, we found that fresher emissions from local sources increased the absorption, which will be discussed in Sect. 3.4.

3.3 Scattering Ångström exponent and single scattering albedo

The long-time averages of the $å_s$ for each pair of wavelengths (450/550 nm, 450/700 nm and 550/700 nm) were nearly equal, between 1.89 and 1.99 (Table 1). The monthly average of the $å_s$ is lowest in the wintertime, decreasing to 1.38 in December 2006 and reaching values of 2.1–2.2 in the summertimes (Fig. 3b).

It must be noted that the $å_s$ values increased, on an average, by 39 % after November 2009 (achieving the maximum value 2.59 in June 2010), when we changed the cut-off size of the interstitial inlet from 2.5 µm to 1.0 µm. This means that fewer coarse particles are nowadays present in the sample, which increases the $å_s$ values, because the dependence of the light scattering on the wavelength of the incident light is stronger for smaller particles. However, we did not observe similar effect on the absolute values of the scattering and absorption coefficients at 550 nm (Fig. 2a-c).

The SSA was lowest in the winter and highest in the summer (Fig. 3c). The average (± 1 standard deviation) SSA was (0.83 ± 0.09), which is comparable to the values of 0.81 observed in in-situ measurements in Northern India (Hyvärinen et al., 2009) and 0.81–0.85 at a rural site near Beijing (Li et al., 2007), but much lower than the SSA values of 0.88 for fine aerosol and 0.96 for coarse aerosol in airborne measurements (Anderson et al., 2003), or the value of 0.98 in a marine environment (Fujitani et al., 2007).

The average value of the SSA measured in-situ at Puijo is rather low compared to those obtained with remote sensing methods (e.g. Dubovik et al., 2002), which provide a columnar SSA. A relatively large aerosol loading is required that the SSA can be retrieved with a reasonable accuracy. For example, in the AERONET (Aerosol Robotic Network) data set, one of the requirements before the SSA measurement can belong to the quality assured (Level 2 data) set, is that the aerosol optical depth (AOD) at 440 nm is greater than 0.4. These kinds of cases are very rare in Kuopio. Therefore, the low SSA value at Puijo can be partly explained by the uncertainty in the SSA, arising from the uncertainties in the scattering and absorption coefficients, and partly by the

sensitivity of the SSA for the scattering coefficient value (Fig. 4). By applying the law for propagation of errors to the relative uncertainties in the scattering coefficient (10 %; Anderson et al., 1996) and absorption coefficient (12 %; Petzold and Schönlinner 2004), we obtained an upper limit of 13 % for the relative uncertainty in the SSA. In Figure 4 the mean values, calculated over bins of $10\,\mathrm{Mm}^{-1}$ of width in $\sigma_{\mathrm{sp},550}$, are presented. The frequency of the $\sigma_{\mathrm{sp},550}$ in each bin decreases dramatically with larger $\sigma_{\mathrm{sp},550}$ values, being 11 356, 4845, 1931, 1015, and 486 for the first five bins and less than 50 after the ninth bin. This frequency distribution puts weight on the lower end of the scattering values, thus lowering the calculated average value. A similar dependence and correlated SSA values averaged over the $10\text{-}\mathrm{Mm}^{-1}$ bins were observed at an anthropogenically influenced continental station by Delene and Ogren (2002). The increase in the SSA with increasing scattering coefficient was confirmed during the the smoke episodes, described above, in July 2010, when the highest monthly average of SSA, 0.91, was observed. During these pollution episodes, the SSA was comparable to the values obtained from sunphotometer measurements carried out at a nearby AERONET (Aerosol Robotic Network) station (Mielonen et al., 2012).

It must be noted that the scattering coefficient at Puijo was measured at relatively dry conditions (RH < 40 %). Therefore, the in-situ SSA value may be underestimated, because the actual scattering coefficient at ambient conditions can be several times larger for the same aerosol than at dry conditions (Zieger et al., 2010). A correction to match the ambient conditions would probably increase the in-situ SSA. However, as we have not determined the so called scattering enhancement factor at Puijo, we can only present the SSA based on the scattering coefficient at dry conditions.

3.4 The effect of local sources on aerosol optical and chemical properties

The $\sigma_{\mathrm{sp},550}$ is highest when the wind blows from the directions of traffic, industry, and residential areas (Table 2). It experiences a local maximum when the wind blows from the northeast, i.e. the direction where the paper mill resides (Fig. 5a). In our earlier study we found that the air masses coming from the north were rich in sulphur dioxide

(Leskinen et al., 2009), which turns fast into sulphate and particulate sulphate, one of the main anthropogenic scattering components.

The $\sigma_{ap,670}$ is largest with southerly winds and above the long-time average of 1.5 Mm^{-1} when the wind blows from the southern highway and larger residential areas (Fig. 5b). These are line and areal sources of diesel particles and emissons from small-scale biomass-fired combustion appliances, respectively. Their emissions contain, among other, soot, which absorbs light efficiently. As expected, we observed the lowest $\sigma_{ap,670}$ with winds from the sector with less local sources (Table 2).

The effect of the the local sources can be seen more clearly from the variation in the SSA and the $\mathring{a}_s$ with the wind direction (Fig. 5c–d). The $\mathring{a}_s$ is larger for the directions of local sources, whose particles are fresh and smaller in size than the aged particles coming from longer distances. The SSA, in turn, is 0.88 when the air masses come from the northeasterly sector, indicating highly scattering aerosol from the paper mill, and 0.81 when the wind blows from the southerly sector (Table 2).

In our AMS analysis we observed a 2–3-fold particulate sulfate concentration with northeasterly winds compared to other wind directions (Fig. 6a). The peak concentration from the direction of the paper mill gives an explanation to the elevated scattering from this direction. The emissions from the south contain 4–5-fold organics than those from the north (Fig. 6b). With northwesterly winds the degree of oxygenation is higher (Fig. 6c), which is due to the oxygenated organics in the aged aerosol particles from the direction with less local sources.

The diurnal variation of the $\sigma_{ap,670}$ and the SSA showed morning (at $\sim$04:00–06:00 a.m. UTC) and afternoon (at $\sim$03:00–05:00 p.m. UTC) peaks in the summer (Fig. 7). This is linked to the increased traffic at these hours. We suggest that in the winter the emissions from traffic are masked by a higher amount of more absorbing particles from other local sources, such as domestic biomass burning appliances. These sources are expected to be active mainly during the daytime and in the evenings. The nightly $\sigma_{ap,670}$ was lower than that in the daytime in all seasons, which resulted also as higher SSA values.

At Puijo the northwesterly sector without local sources matches the West and Arctic sectors defined in the trajectory calculations. The West and Arctic sectors are considered as cleaner than the other sectors including emission sources in Kola Peninsula and the more inhabited Eastern and Southern sectors. Actually, when the wind blows from the northwesterly sector (245–360°), the air masses have spent most of the time (73 %) over the Arctic and West sectors during the last 5 days (Fig. 8) and can be considered as a good background. A similar behaviour with the other local sectors can be seen, i.e. the main trajectory sectors for 0–45°, 45–155°, 155–215°, and 215–245° are Arctic/Kola, East, South, and West, respectively, although there are influences from other sectors, too. Despite this, the influence of the emissions from the Kola Peninsula on the higher SSA values in the 0–45° sector are considered weak, because the air mass trajectories are distributed more evenly with this wind sector, although the main sector is Arctic/Kola (Fig. 8).

3.5 A case study for cloud effects on aerosol optical properties

During the 4-year period, there were altogether 260 cloud events, resulting in 1082 h of in-cloud data. These low-level cloud events occurred mainly in the autumn and early winter, when the relative humidity was at its highest (Fig. 1). The optimal period for investigating low-lever clouds with temperature above 0 °C is September–November (Portin et al., 2009).

We investigated the effect of a cloud event on aerosol optical properties for a four-day period on 7–11 October 2010 (Fig. 9). During this period we observed two cloud events. The first event started on 8 October 2010, 10:45 and lasted 2.5 h, while the second event started on 8 October 2010, 21:45 and lasted 8 h. Before the first cloud event the wind was blowing from the southwestern sectors (200–250°) with residential areas, resulting as a higher $\sigma_{\mathrm{ap},670}$, compared to that observed after the second cloud event, when the wind was blowing from the northwesterly sector (245–360°), with relatively clean and aged aerosol. There was no rain until 10 October 2010, 08:00, i.e. well after the second cloud event.

During the cloud events both the in-cloud and out-of-cloud values for scattering and absorption coefficients decreased (Fig. 9). The effect is stronger for the scattering than for the absorption. The scattering and absorption coefficients of the in-cloud particles are by more than 90 % and 30 % smaller than that of the out-of-cloud particles during the second cloud event, respectively. This results in an approximately 20 % decrease in the SSA. A similar drop in the SSA was observed by Berkowitz et al. (2011) in a foggy situation. The scavenging is less efficient during the first cloud event when there are local, fresher emissions mixed in the sampled air. This is in line with the conclusion by Sellegri et al. (2003) that aging enhances scavenging of carbonaceous aerosols in clouds.

4 Summary and conclusions

We examined aerosol optical properties at a semi-urban measurement station, 230 m above the surroundings, in an observation tower at Puijo in Kuopio, Finland, by measuring light scattering from and absorption into aerosol particles with a three-wavelenght nephelometer and a multi-angle absorption photometer, respectively. By interpreting a four-year data set we were able to determine the annual and diurnal variation of the aerosol scattering and absorption coefficients, single scattering albedo, scattering Ångström exponent and hemispheric backscattering fraction. When we inspected these parameters and results from aerosol mass spectrometry as a function of wind direction, we could see the effect of local sources (a paper mill, traffic, and residential areas) to the aerosol optical and chemical properties. We compared the measured parameters to those obtained in background measurement stations, highly polluted areas, and marine environments, and concluded that Puijo can be regarded as a relatively clean site, regarding the aerosol optical properties. As a case study, we examined how the scattering and absorption coefficient were affected by a cloud event.

In our earlier study (Leskinen et al., 2009) we found that when the wind blows from the northeast, where the paper mill resides, the sulphur dioxide concentration

is elevated. In this study we found that also the sulphate concentration in aerosol particles is higher than at other directions (Fig. 6a). We conclude that the increase in the scattering coefficient and single scattering albedo (Fig. 5a,c) results from the sulphate-rich aerosol from the paper mill, since aerosols containing sulphate are known to be good scatterers of light.

When the wind blows from the sectors with traffic and small scale wood combustion, the single scattering albedo decreases, when the absorption coefficient increases (Fig. 5b,c), and the organic concentration increases (Fig. 6b). We conclude that the air masses from these sectors contained fresh, sooty and organics-rich aerosol from traffic and from small scale biomass combustion in residential biomass-fired appliances. Since the Ångström exponent was larger in the direction of the city center than the residential areas, we conclude that the aerosols emitted by traffic are smaller in size than those in the residential emissions. We conclude that in the wintertime the effect of emissions from the residential areas on absorption is stronger than that from the traffic, because the morning and afternoon peaks in the absorption coefficient, seen in the summertime, are masked by the more absorbing aerosols from the residential areas (Fig. 7a).

We observed increase in the single scattering albedo also when the wind blew from the northwesterly sector with less local sources. From this direction the Ångström exponent was low indicating larger aerosol particles (Fig. 5d). Furthermore, the aerosol mass spectrometry revealed that in this direction there are more oxygenated organic aerosols in the air mass (Fig. 6c). According to the trajectory analysis, most of the air masses with northwesterly wind directions originate from the Arctic region (Fig. 8). Therefore, we conclude that the increase in the SSA arises from the presence of long-range transported aerosol, which are known to be larger in size and more oxygenated than the fresh emissions.

We found that during a cloud event both the in-cloud and out-of-cloud values for scattering and absorption coefficients decreased (Fig. 9), and that the effect is stronger for the scattering (a 90 % decrease) than for the absorption (a 30 % decrease). What

happens to the aerosol optical properties during a cloud event when the air masses come from different directions with different local sources, is under a more detailed inspection. Also, more aerosol mass spectrometry data will be analyzed in order to strengthen our knowledge about the role of the chemical composition of the aerosol particles in their activation into cloud droplets.

References

Aaltonen, V., Lihavainen, H., Kerminen, V.-M., Komppula, M., Hatakka, J., Eneroth, K., Kulmala, M., and Viisanen, Y.: Measurements of optical properties of atmospheric aerosols in Northern Finland, Atmos. Chem. Phys., 6, 1155–1164, doi:10.5194/acp-6-1155-2006, 2006.

Althausen, D., Engelmann, R., Baars, H., Heese, B., Ansmann, A., Müller, D., and Komppula, M.: Portable Raman Lidar Polly(XT) for automated profiling of aerosol backscatter, extinction, and depolarization, J. Atmos. Ocean. Technol., 26, 2366–2378, 2009.

Anderson, T. L. and Ogren, J. A.: Determining aerosol radiative properties using the TSI 3563 integrating nephelometer, Aerosol Sci. Technol., 29, 57–69, 1998.

Anderson, T. L., Covert, D. S., Marshall, S. F., Laucks, M. L., Charlson, R. J., Waggoner, A. P., Ogren, J. A., Caldow, R., Holm, R. L., Quant, F. R., Sem, G. J., Wiedensohler, A., Ahlquist, N. A., and Bates, T. S.: Performance characteristics of a high-sensitivity, three-wavelength, total scatter/backscatter nephelometer, J. Atmos. Ocean. Technol., 13, 967–986, 1996.

Anderson, T. L., Masonis, S. J., Covert, D. S., Ahlquist, N. C., Howell, S. G., Clarke, A. D., and McNaughton, C. S.: Variability of aerosol optical properties derived from in situ aircraft measurements during ACE-Asia, J. Geophys. Res., 108, D8647, doi:10.1029/2002JD003247, 2003.

Andreae, M. O., Schmid, O., Yang, H., Chand, D., Yu, J. Z., Zeng, L.-M., and Zhang, Y.-H.: Optical properties and chemical composition of the atmospheric aerosol in urban Guangzhou, China, Atmos. Environ., 42, 6335–6350, 2008.

Arnott, W. P., Moosmüller, H., Rogers, C. F., Jin, T., and Bruch, R.: Photoacoustic spectrometer for measuring light absorption by aerosol: instrument description, Atmos. Environ., 33, 2845–2852, 1999.

Barriopedro, D., Fischer, E. M., Luterbacher, J., Trigo, R. T., and García-Herrera, R.: The hot summer of 2010: redrawing the temperature record map of Europe, Science, 332, 220–224, doi:10.1126/science.1201224, 2011.

Baynard, T., Lovejoy, E. R., Petterson, A., Brown, S. S., Lack, D., Osthoff, H., Massoli, P., Ciciora, S., Dube, W. P., and Ravishankara, A. R.: Design and application of a pulsed cavity ring-down aerosol extinction spectrometer for field measurements, Aerosol Sci. Technol., 41, 447–462, 2007.

Bergin, M. H., Cass, G. R., Xu, J., Fang, C., Zeng, L. M., Yu, T., Salmon, L. G., Kiang, C. S., Tang, X. Y., Zhang, Y. H., and Chameides, W. L.: Aerosol radiative, physical, and chemical properties in Beijing during June 1999, J. Geophys. Res.-Atmos., 106, 17969–17980, 2001.

Berkowitz, C. M., Berg, L. K., Yu, X.-Y., Alexander, M. L., Laskin, A., Zaveri, R. A., Jobson, B. T., Andrews, E., and Ogren, J. A.: The influence of fog and airmass history on aerosol optical, physical and chemical properties at Pt. Reyes National Seashore, Atmos. Environ., 45, 2559–2568, 2011.

Bohren, C. F. and Huffman, D. R. (Eds.): Absorption and scattering of light by small particles, John Wiley, New York, N. J., USA, 1983.

Chen, G., Ziemba, L. D., Chu, D. A., Thornhill, K. L., Schuster, G. L., Winstead, E. L., Diskin, G. S., Ferrare, R. A., Burton, S. P., Ismail, S., Kooi, S. A., Omar, A. H., Slusher, D. L., Kleb, M. M., Reid, J. S., Twohy, C. H., Zhang, H., and Anderson, B. E.: Observations of Saharan dust microphysical and optical properties from the Eastern Atlantic during NAMMA airborne field campaign, Atmos. Chem. Phys., 11, 723–740, doi:10.5194/acp-11-723-2011, 2011.

Delene, D. J. and Ogren, J. A.: Variability of aerosol optical properties at four North American surface monitoring sites, J. Atmos. Sci., 59, 1135–1150, 2002.

Dubovik, O., Holben, B., Eck, T. F., Smirnov, A., Kaufman, Y. J., King, M. D., Tanré, D., and Slutsker, I.: Variability of absorption and optical properties of key aerosol types observed in worldwide locations, J. Atmos. Sci., 59, 590–608, 2002.

Fierz-Schmidhauser, R., Zieger, P., Wehrle, G., Jefferson, A., Ogren, J. A., Baltensperger, U., and Weingartner, E.: Measurement of relative humidity dependent light scattering of aerosols, Atmos. Meas. Tech., 3, 39–50, doi:10.5194/amt-3-39-2010, 2010.

Fischer, E. V., Jaffe, D. A., Marley, N. A., Gaffney, J. S., and Marchany-Rivera, A.: Optical

properties of aged Asian aerosols observed over the U.S. Pacific Northwest, J. Geophys. Res., 115, D20209, doi:10.1029/2010JD013943, 2010.

Fujitani, Y., Murao, N., Ohta, S., Endoh, T., Yamagata, S.: Optical and chemical properties of marine aerosols over the central equatorial Pacific Ocean during the 2003 R/V Mirai cruise, J. Geophys. Res., 112, D11213, doi:10.1029/2006JD008354, 2007.

He, X., Li, C. C., Lau, A. K. H., Deng, Z. Z., Mao, J. T., Wang, M. H., Liu, X. Y.: An intensive study of aerosol optical properties in Beijing urban area, Atmos. Chem. Phys, 9, 8903–8915, doi:10.5194/acp-9-8903-2009, 2009.

Heintzenberg, J. and Charlson, R. J.: Design and applications of the integrating nephelometer: a review, J. Atmos. Ocean. Technol., 13, 987–1000, 1996.

Hyvärinen, A.-P., Lihavainen, H., Komppula, M., Sharma, V. P., Kerminen, V.-M., Panwar, T. S., and Viisanen, Y.: Continuous measurements of optical properties of atmospheric aerosols in Mukteshwar, northern India, J. Geophys. Res., 114, D08207, doi:10.1029/2008JD011489, 2009.

Hänel, G.: Vertical profiles of the scattering coefficient of dry atmospheric particles over Europe normalized to air at standard temperature and pressure, Atmos. Environ., 32, 1743–1755, 1998.

IPCC (Intergovernmental Panel on Climate Change): Climate Change 2007 – The Physical Science Basis, edited by: Solomon, S., Cambridge Univ. Press, New York, USA, 2007.

Jayne, J., Leard, D., Zhang, X., Davidovits, P., Smith, K., Kolb, C., and Worsnop, D.: Development of an aerosol mass spectrometer for size and composition analysis of submicron particles, Aerosol Sci. Technol., 22, 49–70, 2000.

Knox, A., Evans, G. J., Brook, J. R., Yao, X., Jeong, C.-H., Godri, K. J., Sabaliauskas, K., and Slowik, J. G.: Mass absorption cross-section of ambient black carbon aerosol in relation to chemical age, Aerosol Sci. Technol., 43, 522–532, 2009.

Leskinen, A., Portin, H., Komppula, M., Miettinen, P., Arola, A., Lihavainen, H., Hatakka, J., Laaksonen, A., and Lehtinen, K. E. J.: Overview of the research activities and results at Puijo semi-urban measurement station, Boreal Env. Res., 14, 576–590, 2009.

Li, C., Marufu, L. T., Dickerson, R. R., Li, Z., Wen, T., Wang, Y., Wang, P., Chen, H., and Stehr, J. W.: In situ measurements of trace gases and aerosol optical properties at a rural site in northern China during East Asian Study of Tropospheric Aerosols: An International Regional Experiment 2005, J. Geophys. Res., 112, D22S04, doi:10.1029/2006JD007592, 2007.

Marcq, S., Laj, P., Roger, J. C., Villani, P., Sellegri, K., Bonasoni, P., Marinoni, A., Cristofanelli,

P., Verza, G. P., and Bergin, M.: Aerosol optical properties and radiative forcing in the high Himalaya based on measurements at the Nepal Climate Observatory-Pyramid site (5079 m a.s.l.), Atmos. Chem. Phys., 10, 5859–5872, doi:10.5194/acp-10-5859-2010, 2010.

Mielonen, T., Portin, H., Komppula, M., Leskinen, A., Tamminen, J., Ialongo, I., Hakkarainen, J., Lehtinen, K. E. J., and Arola, A.: Biomass burning aerosols observed in Eastern Finland during the Russian wild-fires in summer 2010 – Part 2: Remote sensing, Atmos. Environ., 47, 279–287, 2012.

Pandolfi, M., Cusack, M., Alastuey, A., and Querol, X.: Variability of aerosol optical properties in the Western Mediterranean Basin, Atmos. Chem. Phys., 11, 8189–8203, doi:10.5194/acp-11-8189-2011, 2011.

Petzold, A. and Schönlinner, M.: Multi-angle absorption photometry – a new method for the measurement of aerosol light absorption and atmospheric black carbon, J. Aerosol Sci., 35, 421–441, 2004.

Portin, H. J., Komppula, M., Leskinen, A. P., Romakkaniemi, S., Laaksonen, A., and Lehtinen, K. E. J.: Observations of aerosol-cloud interactions at the Puijo semi-urban measurement station, Boreal Env. Res., 14, 641–653, 2009.

Portin, H., Mielonen, T., Leskinen, A., Arola, A., Pärjälä, E., Romakkaniemi, S., Laaksonen, A., Lehtinen, K. E. J., and Komppula, M.: Biomass burning aerosols observed in Eastern Finland during the Russian wildfires in summer 2010 – Part 1: In-situ aerosol characterization, Atmos. Environ., 47, 269–278, 2012.

Sellegri, K., Laj, P., Dupuy, R., Legrand, M., Preunkert, S., and Putaud, J.-P.: Size-dependent scavenging efficiencies of multicomponent atmospheric aerosols in clouds, J. Geophys. Res., 108, 4334, doi:10.1029/2002JD002749, 2003.

Shinozuka, Y., Redemann, J., Livingston, J. M., Russell, P. B., Clarke, A. D., Howell, S. G., Freitag, S., O'Neill, N. T., Reid, E. A., Johnson, R., Ramachandran, S., McNaughton, C. S., Kapustin, V. N., Brekhovskikh, V., Holben, B. N., and McArthur, L. J. B.: Airborne observation of aerosol optical depth during ARCTAS: vertical profiles, inter-comparison and fine-mode fraction, Atmos. Chem. Phys., 11, 3673–3688, doi:10.5194/acp-11-3673-2011, 2011.

Shiraiwa, M., Kondo, Y., Iwamoto, T., and Kita, K.: Amplification of light absorption of black carbon by organic coating, Aerosol Sci. Technol., 46–54, 2010.

Stohl, A., Wotawa, G., Seibert, P., and Kromp-Kolb, H.: Interpolation errors in wind fields as a function of spatial and temporal resolution and their impact on different types of kinematic trajectories, J. Appl. Meteor., 34, 2149–2165, 1995.

Title Page

Abstract | Introduction

Conclusions | References

Tables | Figures

⏮ | ⏭

◀ | ▶

Back | Close

Full Screen / Esc

Printer-friendly Version

Interactive Discussion

Virkkula, A., Backman, J., Aalto, P. P., Hulkkonen, M., Riuttanen, L., Nieminen, T., dal Maso, M., Sogacheva, L., de Leeuw, G., and Kulmala, M.: Seasonal cycle, size dependencies, and source analyses of aerosol optical properties at the SMEAR II measurement station in Hyytiälä, Finland, Atmos. Chem. Phys., 11, 4445–4468, doi:10.5194/acp-11-4445-2011, 2011.

Weingartner, E., Nyeki, S., and Baltensperger, U.: Seasonal and diurnal variation of aerosol size distributions ($10 < D < 750$ nm) at a high-alpine site (Jungfraujoch 3580 m a.s.l.), J. Geophys. Res., 104, 26809–26820, 1999.

Zieger, P., Fierz-Schmidhauser, R., Gysel, M., Ström, J., Henne, S., Yttri, K. E., Baltensperger, U., and Weingartner, E.: Effects of relative humidity on aerosol light scattering in the Arctic, Atmos. Chem. Phys., 10, 3875–3890, doi:10.5194/acp-10-3875-2010, 2010.

Title Page

Abstract | Introduction

Conclusions | References

Tables | Figures

◄ | ►

◄ | ►

Back | Close

Full Screen / Esc

Printer-friendly Version

Interactive Discussion

Table 1. Number (N), mean, standard deviation (std), 10th, 50th, and 90th percentiles, and maxima (max) of valid observations for aerosol scattering and backscattering coefficients at 450, 550, and 700 nm ($\sigma_{sp,450}$, $\sigma_{bsp,450}$, $\sigma_{sp,550}$, $\sigma_{bsp,550}$, $\sigma_{sp,700}$, and $\sigma_{bsp,700}$ in Mm^{-1}), hemispheric backscattering fractions at 450, 550, and 700 nm (b_{450}, b_{550}, and b_{700}), Ångström exponents between 550 and 450 nm, 700 and 450 nm, and 700 and 550 nm ($å_{s,550-450}$, $å_{s,700-450}$, $å_{s,700-550}$), absorption coefficient at 670 nm ($\sigma_{ap,670}$ in Mm^{-1}) and single scattering albedo at 670 nm (SSA$_{670}$) based on hourly averages.

parameter	N	mean	std	percentiles 10	50	90	max
$\sigma_{sp,450}$	20 175	16.4	19.4	3.2	10.3	36.5	412.9
$\sigma_{sp,550}$	20 175	11.1	13.5	2.2	7.0	24.5	315.4
$\sigma_{sp,700}$	20 175	6.8	8.5	1.4	4.4	14.6	229.6
$\sigma_{bsp,450}$	2435	3.3	4.0	0.7	1.8	7.7	42.0
$\sigma_{bsp,550}$	2435	2.3	3.0	0.4	1.2	5.6	31.9
$\sigma_{bsp,700}$	2435	2.3	2.9	0.4	1.3	5.1	30.2
b_{450}	2377	0.11	0.03	0.08	0.11	0.15	N/A*
b_{550}	2681	0.13	0.04	0.09	0.12	0.17	N/A
b_{700}	1823	0.16	0.10	0.11	0.15	0.22	N/A
$å_{s,550-450}$	20175	1.89	0.46	1.30	1.95	2.35	4.58
$å_{s,700-450}$	20 175	1.95	0.50	1.26	2.03	2.42	7.08
$å_{s,700-550}$	20 175	1.99	0.61	1.20	2.09	2.52	9.20
$\sigma_{ap,670}$	28 405	1.5	1.6	0.3	0.9	3.2	36.5
SSA$_{670}$	19 946	0.83	0.09	0.71	0.84	0.92	1.00

*N/A = not available.

Table 2. The averages of the aerosol optical parameters over the chosen sectors with emission sources: highway, paper mill, city center, district heating plant, and residential areas (RA) extending up to 10 km. Please see caption of Table 1 for explanation of the parameters.

sector	highway and paper mill, 0–45°	RA (0–4 km) and city center, 45–155°	RA (0–10 km) and district heating plant, 155–215°	RA (0–4 km), 215–245°	RA (0–3 km), 245–360°
$\sigma_{sp,450}$	24.0	23.6	24.7	19.1	13.9
$\sigma_{sp,550}$	17.1	16.0	17.0	13.1	9.4
$\sigma_{sp,700}$	10.2	9.4	10.2	7.8	5.6
$\sigma_{bsp,450}$	1.6	2.9	3.1	3.4	1.7
$\sigma_{bsp,550}$	1.1	2.1	2.2	2.5	1.1
$\sigma_{bsp,700}$	1.1	2.0	2.3	2.4	1.2
b_{450}	0.11	0.11	0.12	0.11	0.11
b_{550}	0.12	0.13	0.13	0.12	0.12
b_{700}	0.16	0.16	0.17	0.15	0.16
$å_{s,550-450}$	1.85	1.98	1.91	1.80	1.84
$\sigma_{ap,670}$	1.2	1.9	2.2	1.4	0.9
SSA_{670}	0.88	0.83	0.81	0.85	0.87
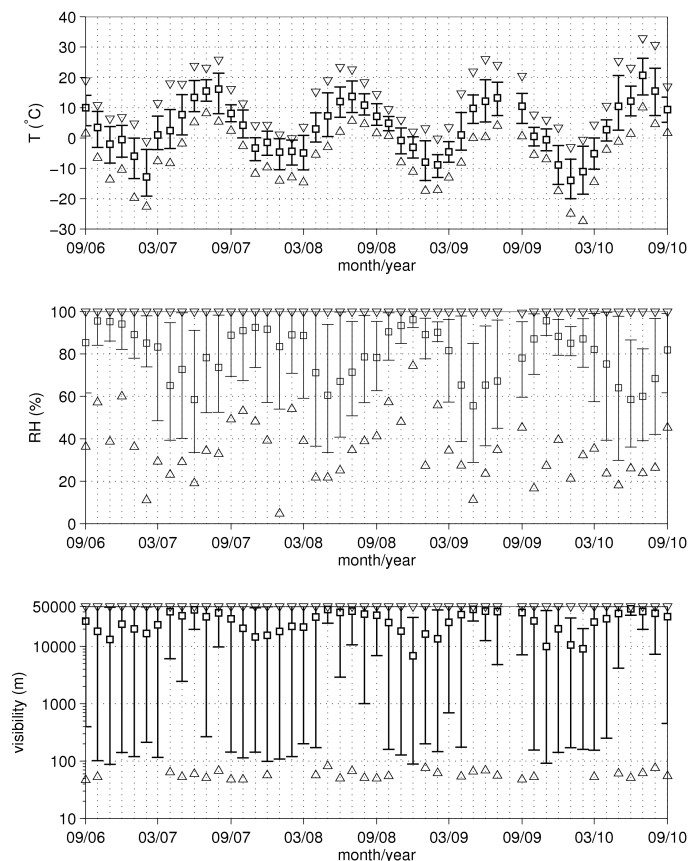
Fig. 1. Monthly minimum (triangle up), 10th percentile (lower error bar), mean (square), 90th percentile (upper error bar), and maximum (triangle down) of **(a)** temperature, **(b)** relative humidity, and **(c)** horizontal visibility at Puijo in Sep 2006–Sep 2010.
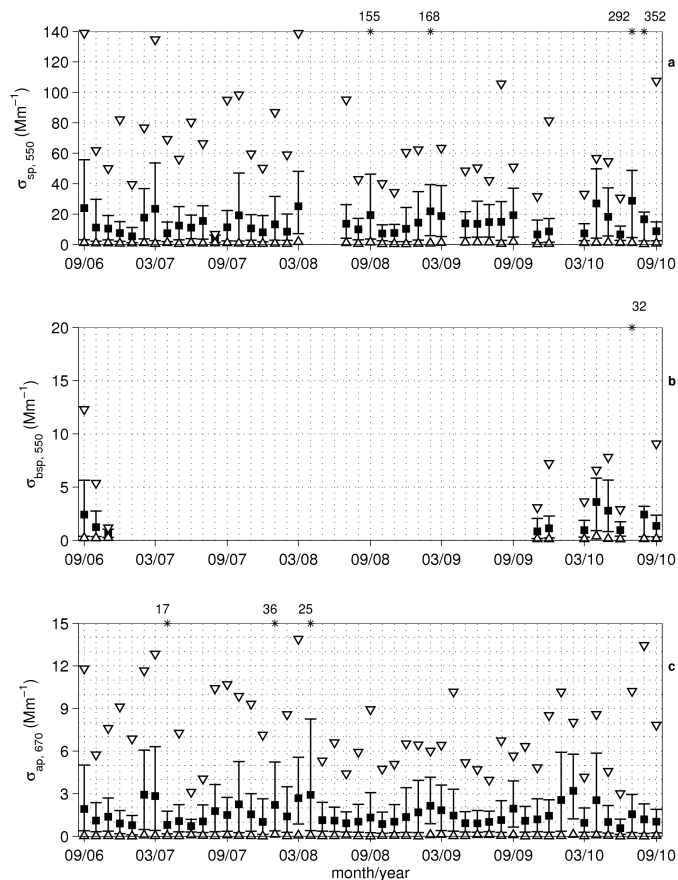
Fig. 2. Monthly minimum (triangle up), 10th percentile (lower error bar), mean (square), 90th percentile (upper error bar), and maximum (triangle down or star with the maximum value) of **(a)** total scattering coefficient at 550 nm, **(b)** back scattering coefficient at 550 nm, and **(c)** absorption coefficient at 670 nm at Puijo in Sep 2006–Sep 2010.

Title Page

Abstract | Introduction

Conclusions | References

Tables | Figures

◀ | ▶

◀ | ▶

Back | Close

Full Screen / Esc

Printer-friendly Version

Interactive Discussion
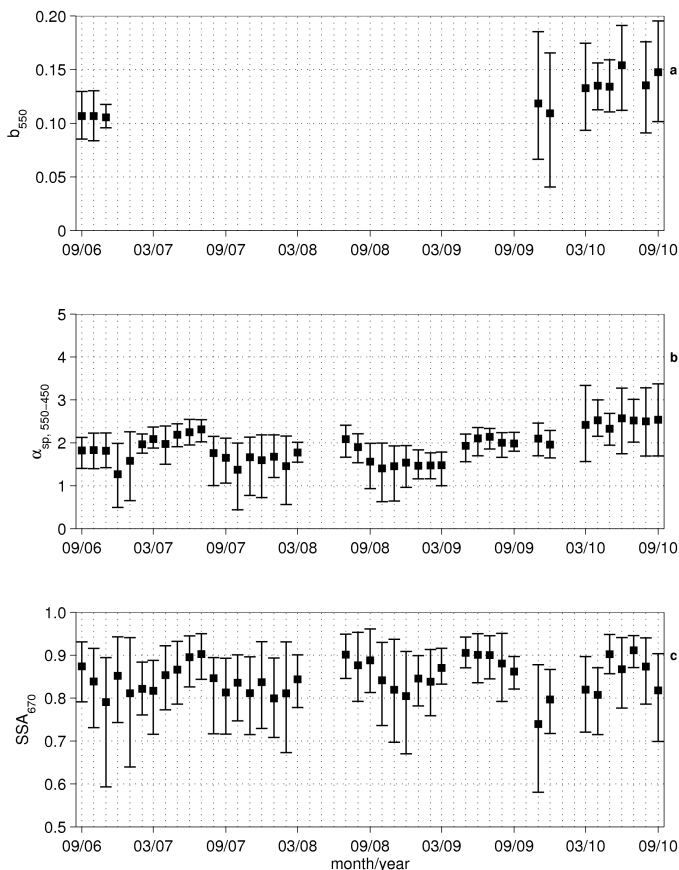
Fig. 3. Monthly averages of hemispheric backscattering fraction at 550 nm **(a)**, scattering Ångström exponent between 450 and 550 nm **(b)**, and single scattering albedo at 670 nm **(c)** at Puijo in Sep 2006–Sep 2010.
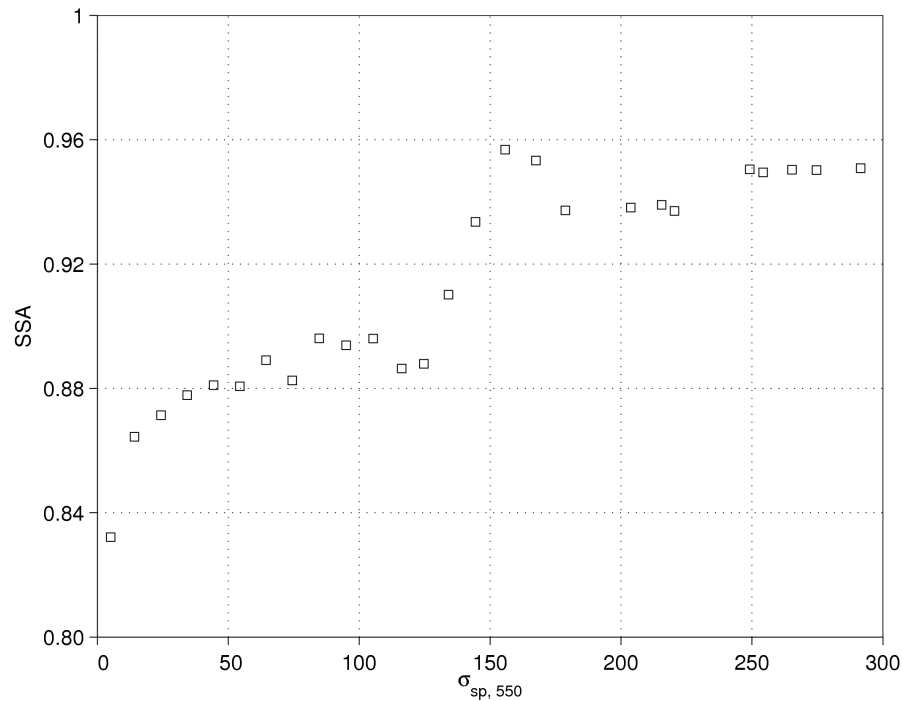
Fig. 4. Mean single scattering albedo (SSA) classified according to 10-Mm^{-1} bins of the scattering coefficient at 550 nm ($s_{sp,550}$).
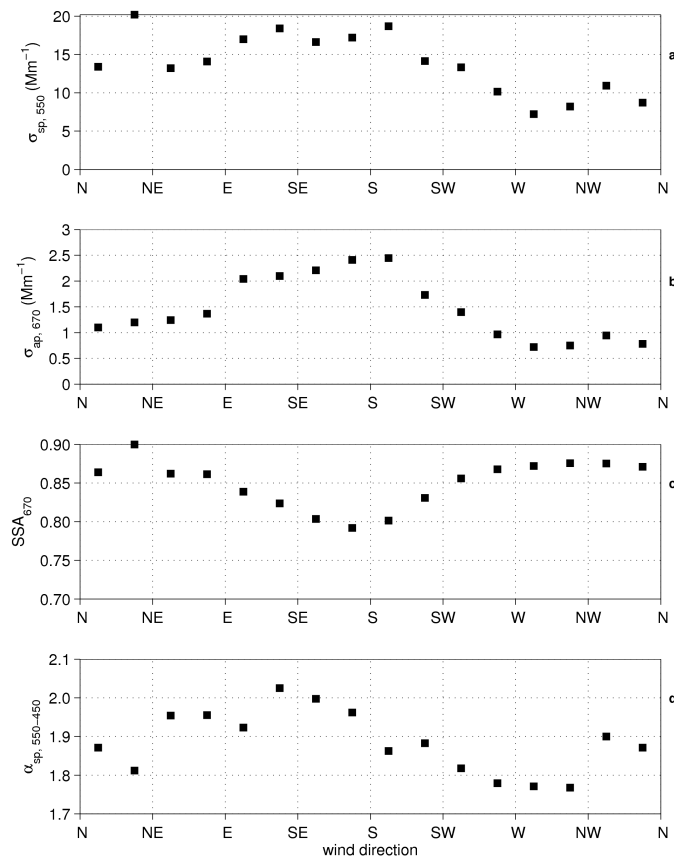
Fig. 5. The average total scattering coefficient at 550 nm **(a)**, absorption coefficient at 670 nm **(b)**, single scattering albedo at 670 nm **(c)**, and scattering Ångström exponent between 450 and 550 nm **(d)** as a function of wind direction at Puijo in Sep 2006–Sep 2010.

Title Page

Abstract | Introduction

Conclusions | References

Tables | Figures

◄ | ►

◄ | ►

Back | Close

Full Screen / Esc

Printer-friendly Version

Interactive Discussion
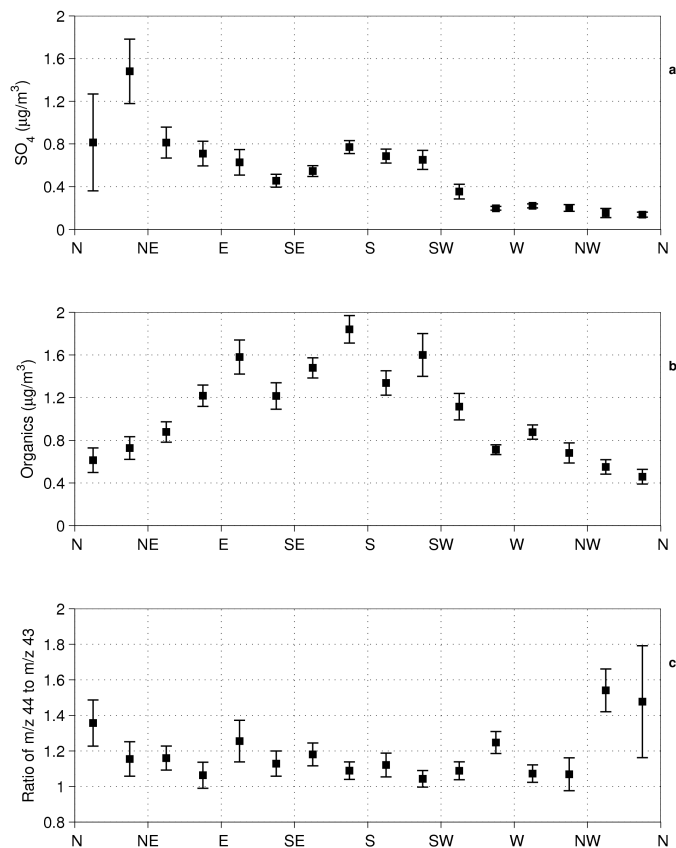
Fig. 6. The **(a)** sulphate concentration, **(b)** organics concentration, and **(c)** the ratio of mass numbers 44 to 43 in non-refractory submicron particles as a function of compass point at Puijo, averaged over time period of 16 Sep–20 Oct 2008. The error bars indicate the standard error of mean.
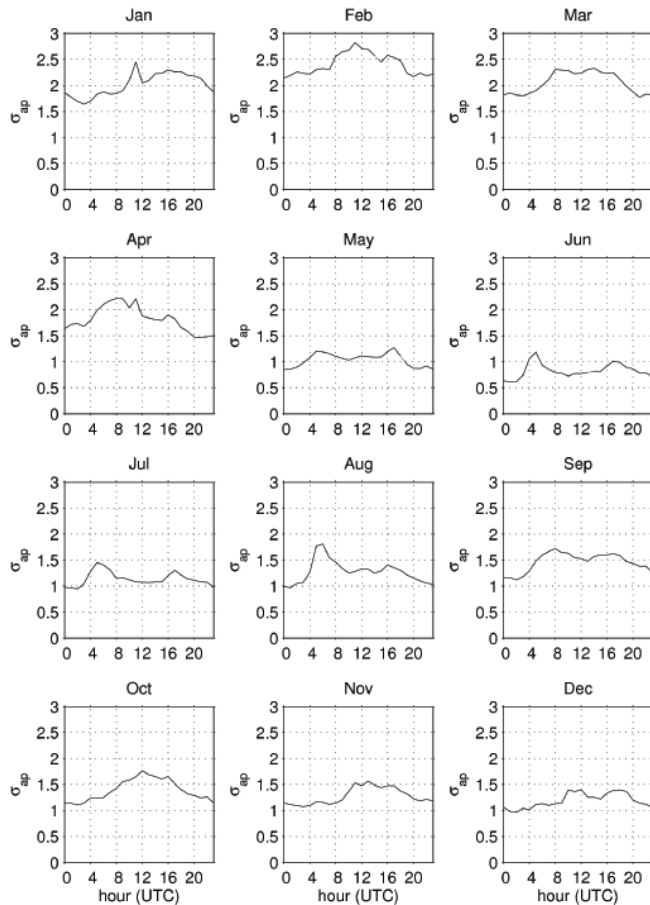
a

Fig. 7a. The **(a)** absorption coefficient at 670 nm and **(b)** single scattering albedo as a function of hour and month at Puijo. The months of the years 2006–2010 were combined.

Fig. 7b. Continued.

Title Page

Abstract | Introduction

Conclusions | References

Tables | Figures

◄ | ►|

◄ | ►

Back | Close

Full Screen / Esc

Printer-friendly Version

Interactive Discussion
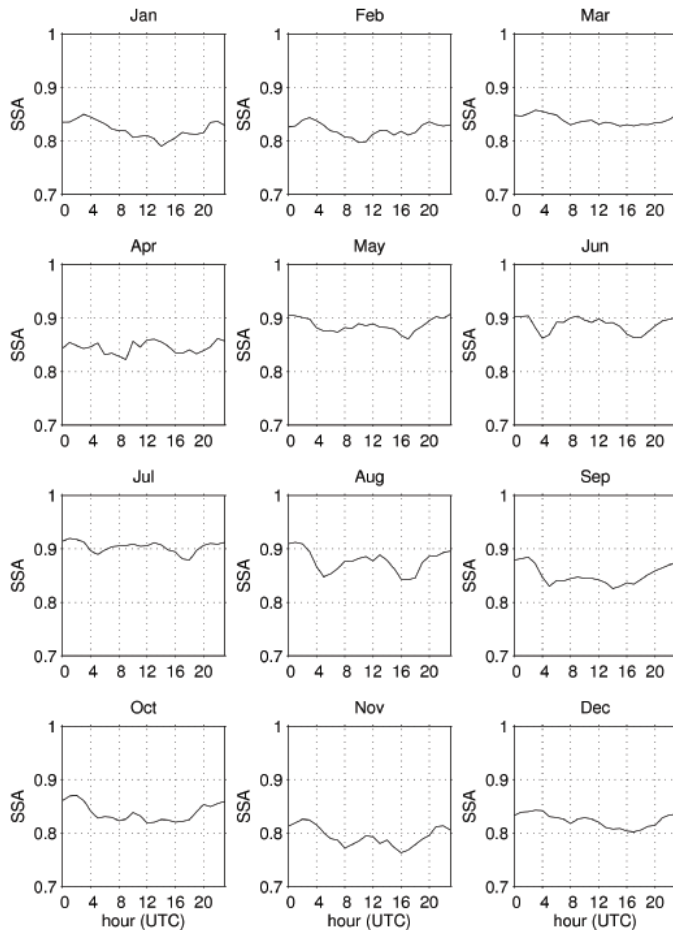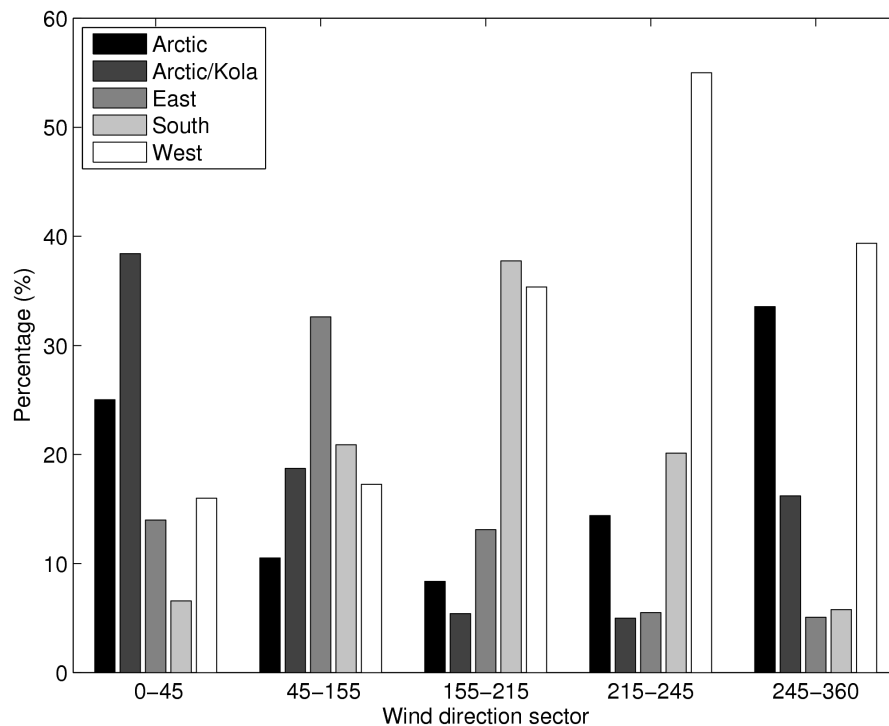
Fig. 8. The distribution of air mass origins (trajectory sectors) with each local source sector.
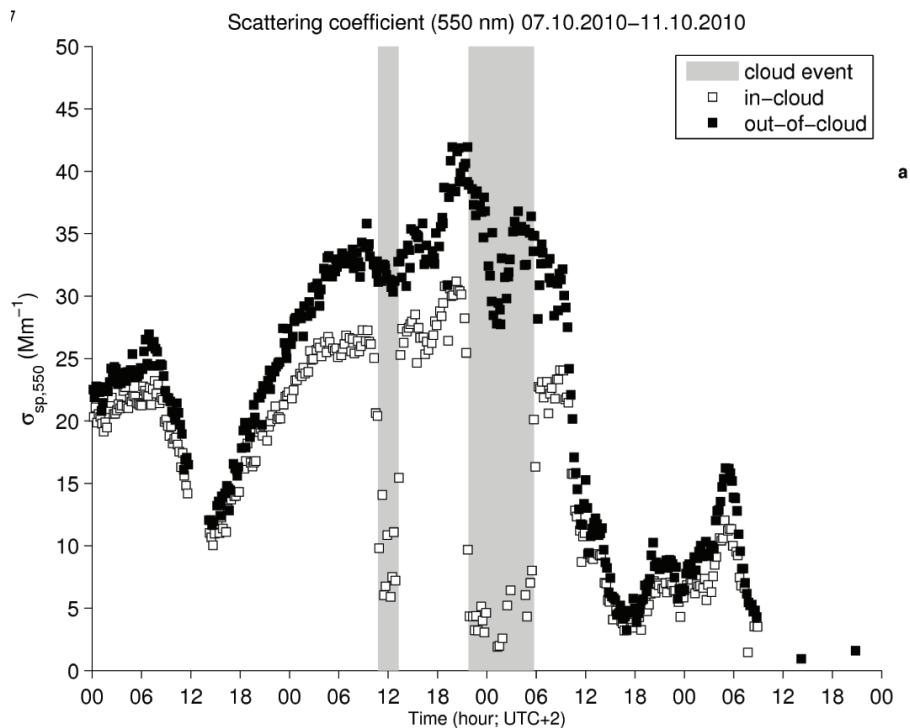
Fig. 9a. The **(a)** total scattering coefficient at 550 nm and **(b)** absorption coefficient at 670 nm of total (out-of-cloud) and interstitial (in-cloud) aerosol particles at Puijo 7–11 Oct 2010, when two cloud events took place.

Fig. 9b. Continued.

Title Page

Abstract | Introduction

Conclusions | References

Tables | Figures

◄ | ►

◄ | ►

Back | Close

Full Screen / Esc

Printer-friendly Version

Interactive Discussion